Electronic Supplementary Material (ESI) for New Journal of Chemistry.

Supporting Information

Two new transition metal-organic frameworks as multiresponsive fluorescence sensors for detecting Fe^{3+}, $Cr_2O_7^{2-}$ and TNP

Jun-Jun Li,[a,b] Zhen-Jie Feng,[a,b] Xue-Song Wu,*[a,b] Ying-Li,[a,b] Di Wu,[a,b] Jing Sun,*[a,b] Xin-Long Wang[a,c] and Zhong-Min Su*[a,b,d]

[a] Jilin Provincial Science and Technology Innovation Center of Optical Materials and Chemistry, School of Chemistry and Environmental Engineering, Changchun University of Science and Technology, Changchun, 130022, People's Republic of China

[b] Jilin Provincial International Joint Research Center of Photo-functional Materials and Chemistry, Changchun, 130022, People's Republic of China

[c] National & Local United Engineering Laboratory for Power Battery Institution, Northeast Normal University, Changchun, Jilin, 130024, People's Republic of China

[d] College of Chemistry, Jilin University, Changchun, 130012, People's Republic of China

*Corresponding Author E-mail: wxs@cust.edu.cn (X.-S. Wu); sj-cust@126.com (J. Sun); zmsu@nenu.edu.cn (Z.-M. Su).

Chemicals and instrumentations.

3, 5-bis(imidazole-1-yl)pyridine (Bip) was prepared under laboratory conditions according to references[1], while other reagents and solvents were obtained commercially and used without further purification. The FT-IR spectra were carried out on a Nicolet Magna 750 FTIR spectrometer using KBr pellets in the range of 4000-400 cm^{-1}. The UV-vis absorption spectra were measured and obtained with a Varian Cary 50 spectrophotometer. Thermal gravimetric analysis (TGA) was performed on a EVO2G-TG-08 analyzer in a nitrogen atmosphere with a temperature range of 35-800 °C and a heating rate of 10°C min^{-1}. Powder X-ray diffraction (PXRD) patterns were obtained on a Rigaku Smart Lab with Cu-Kα (λ = 1.5418 Å) radiation in the range 5-50°. Solid state fluorescence and all fluorescence sensing experiments were carried out on a F-7000 fluorescence spectrometer.

X-ray crystallography.

The single-crystal X-ray diffraction measurements of all crystals were performed on a Bruker Axs Apex III CCD diffractometer equipped with graphite monochromated Mo-Ka radiation (λ =0.71073 Å). The data of crystals were collected at room temperature. Multi-scan absorption corrections were applied using the SADABS program. The structure of crystals was solved by direct methods and refined by F^2 full-matrix refinement using the SHELXTL package (SHELXTL-97). The detail single-crystal data of **CUST-751** and **CUST-752** are showed in Table 1. The selected bond lengths (Å) are presented in Table S1-S2. The CCDC numbers of **CUST-751** and **CUST-752** are 2171855 and 2171856, respectively.

Luminescence sensing experiments.

The whole process of the experiments was manipulated at room temperature. DMF was chosen as the solvent, and the long-term stability of MOFs in DMF could be proved in Fig. S6-S7.

Sensing of cations and anions.

The as-synthesized **CUST-751** and **CUST-752** were finely ground for sensing tests.

For each test, a ground sample (2 mg) was dispersed into different DMF solutions (2 mL, 1.0 mmol·L^{-1}) containing $M(NO_3)_x$ (M = Al^{3+}, Ba^{2+}, Ca^{2+}, Cd^{2+}, Cr^{3+}, Cu^{2+}, Co^{2+}, K^+, Hg^{2+}, Mg^{2+}, Na^+, Ni^{2+}, Zn^{2+} and Fe^{3+}) or KX (X = F^-, Cl^-, Br^-, I^-, CH_3COO^-, $H_2PO_4^-$, BrO_3^-, OH^-, CO_3^{2-}, HPO_4^{2-}, CrO_4^{2-}, and $Cr_2O_7^{2-}$). DMF suspensions of **CUST-751** and **CUST-752** were obtained by ultrasound for 30 min. The anti-interference experiments were carried out to verify the sensitivity in the presence of Fe^{3+} and other interfering metal ions with an equal concentration in DMF (1.0 mmol·L^{-1}).

Sensing of nitroaromatic explosives.

Dissolve the analyte in DMF and prepare it into a solution with different concentrations. Then take 2 mL of the solution and add it into the sample tube containing 2 mg of crystal powder. After ultrasonic treatment for 30 min, disperse it evenly and form a stable suspension. Let it stand for 1 min. Test it by fluorescence spectrometer to check the quenching condition of the material. Check the selective quenching of different analytes according to the quenching condition of the material.

Computational details.

The fluorescence quenching was analyzed using the Stern-Volmer equations:

$$I_0/I = 1 + K_{SV} [M]$$

where I_0 and I are the fluorescence intensity, in the absence and presence of analyte, respectively, K_{SV} is the Stern-Volmer quenching constant and [M] is the concentration of analyte.

The quenching percentage was calculated using the equation as follows:

$$\text{Fluorescence quenching\%} = (1 - I/I_0) \times 100\%$$

where I_0 is the initial fluorescence intensity in the absence of metal ions, I is the fluorescence intensity in the presence of corresponding analyte.

The limit of detection concentration (LOD) was calculated according to the formula:

$$LOD = 3\sigma / K_{SV}$$

and σ is the standard deviation of the detection method.

Recyclable luminescence experiments.

After the first fluorescence detection of various analytes, the powder samples of

CUST-751 and **CUST-752** were recovered by centrifugation and washed by DMF. After drying, the samples collected were used again for the detection of various analytes.

Table S1. Selected bond length (Å) for **CUST-751.**

Bond	**length (Å)**	**Bond**	**length (Å)**
Zn1-O8	2.018(16)	Zn2-O2	1.94(2)
Zn1-O10	2.229(19)	Zn2-N5	1.922(13)
Zn1-N6	1.990(13)	Zn3-O12	1.969(17)
Zn1-N15	1.985(12)	Zn3-O11	2.131(17)
Zn1-N1^{1}	2.15(2)	Zn3-N11	1.943(13)
Zn2-O3	1.91(2)	Zn3-N10	1.976(13)
Zn2-O1	1.99(2)	Zn3-N3^{2}	2.3(2)
Symmetry transformations used to generate equivalent atoms: ^{1}1+X, +Y, -1+Z; ^{2}1-X, -1/2+Y, 1-Z; ^{3}-1+X, +Y, 1+Z; ^{4}1-X, 1/2+Y, 1-Z.			

Table S2. Selected bond length (Å) for **CUST-752.**

Bond	**length (Å)**	**Bond**	**length (Å)**
Cd1-O1^{1}	2.490(4)	Cd2-O5^{3}	2.355(5)
Cd1-O2	2.481(4)	Cd2-O5	2.355(5)
Cd1-O3^{3}	2.265(4)	Cd2-O6^{4}	2.356(4)
Cd1-N1	2.223(4)	Cd2-O6^{5}	2.356(4)
Cd1-O4	2.250(4)	Cd2-N5^{3}	2.238(5)
Cd1-O7	2.363(4)	Cd2-N5	2.238(5)
Symmetry transformations used to generate equivalent atoms: ^{1}2-X, 1-Y, 1-Z; ^{2}+X,1+Y, +Z; ^{3}-X, 2-Y, 2-Z; ^{4}1-X, 1-Y, 1-Z; ^{5}-1+X, 1+Y, 1+Z; ^{6}+X, -1+Y, +Z; ^{7}1+X, -1+Y, -1+Z.			

Characterizations and results.

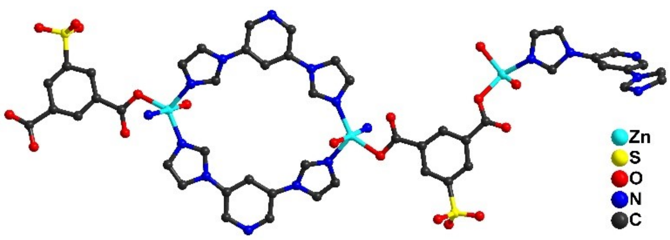

Fig. S1 Asymmetric unit of **CUST-751** (all hydrogen atoms are omitted for clarity).

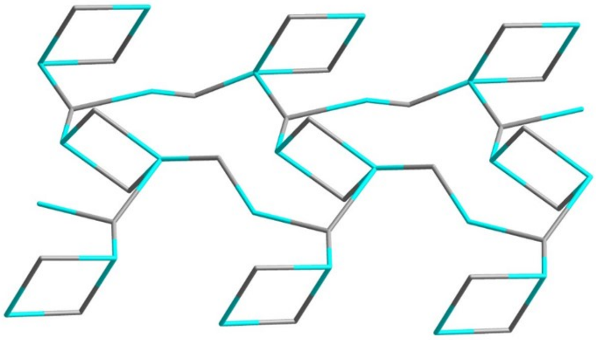

Fig. S2 The cluster simplification of **CUST-751** in ToposPro.

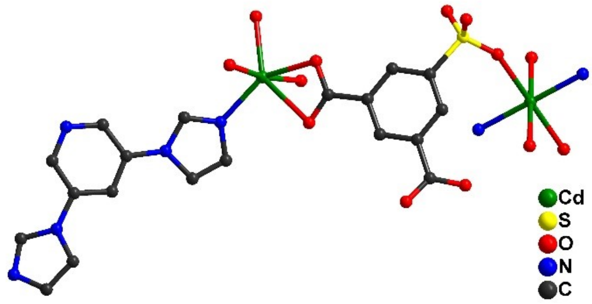

Fig. S3 Asymmetric unit of **CUST-752** (all hydrogen atoms are omitted for clarity).

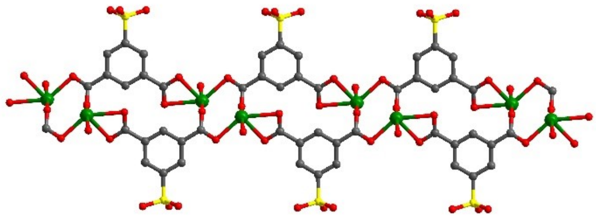

Fig. S4 1D chain formed by binuclear $[Cd_2(COO)_2]$ units.

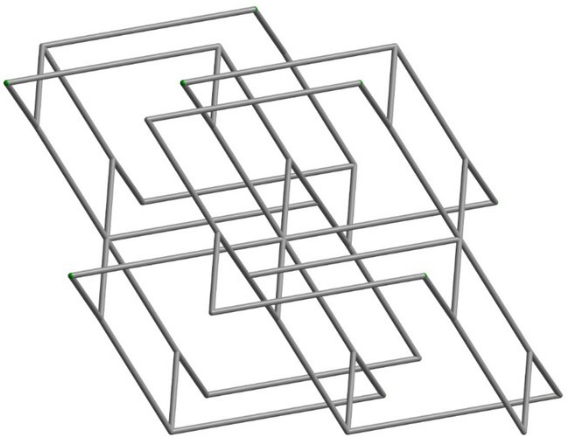

Fig. S5 The cluster simplification of **CUST-752** in ToposPro.

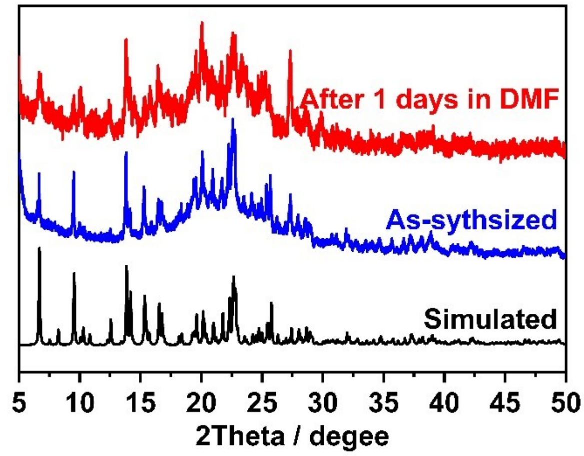

Fig. S6 Powder X-ray diffraction patterns of **CUST-751.**

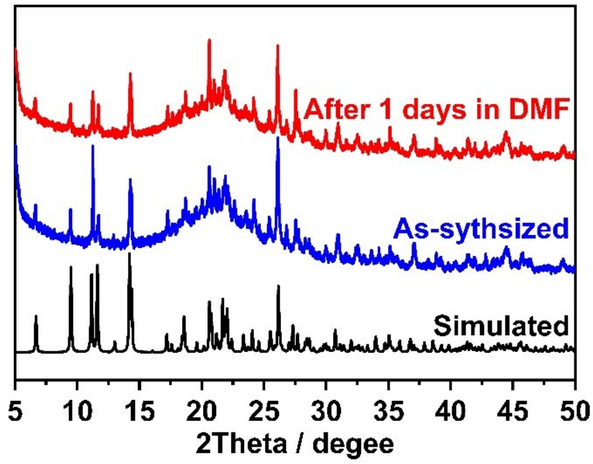

Fig. S7 Powder X-ray diffraction patterns of **CUST-752.**

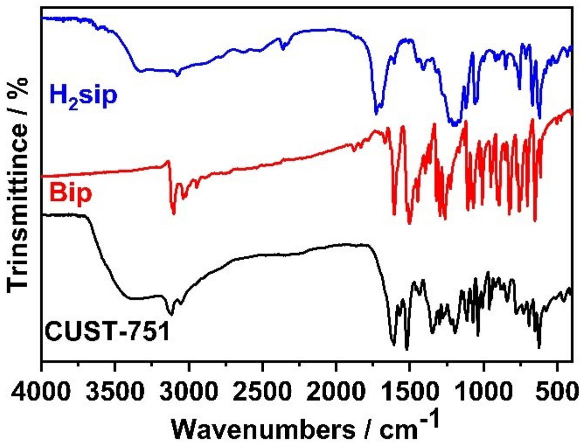

Fig. S8 The IR spectrum of **CUST-751**, Bip and H_2sip.

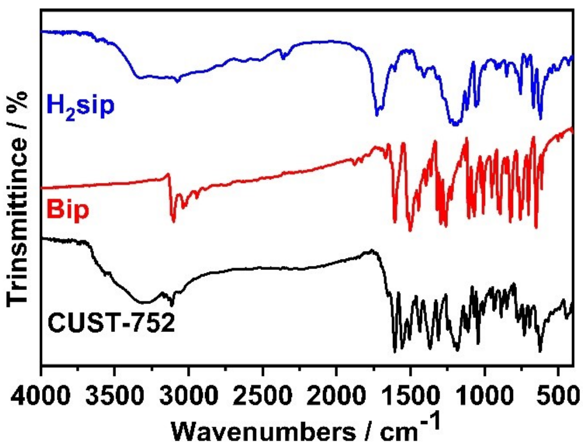

Fig. S9 The IR spectrum of **CUST-752**, Bip and H_2sip.

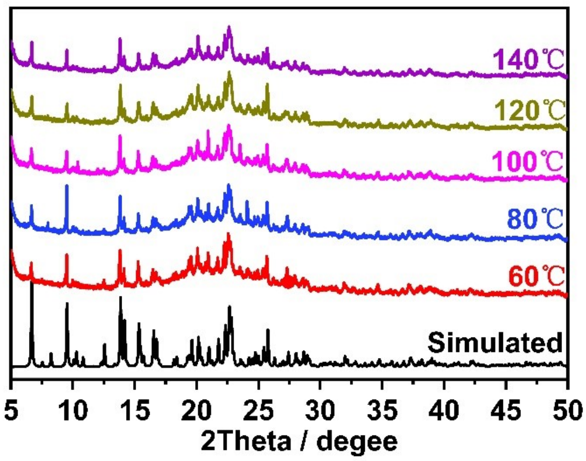

Fig. S10 Variable temperature PXRD patterns of **CUST-751**.

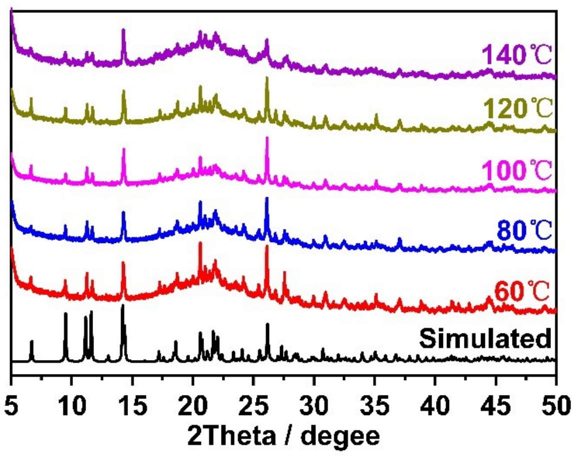

Fig. S11 Variable temperature PXRD patterns of **CUST-752**.

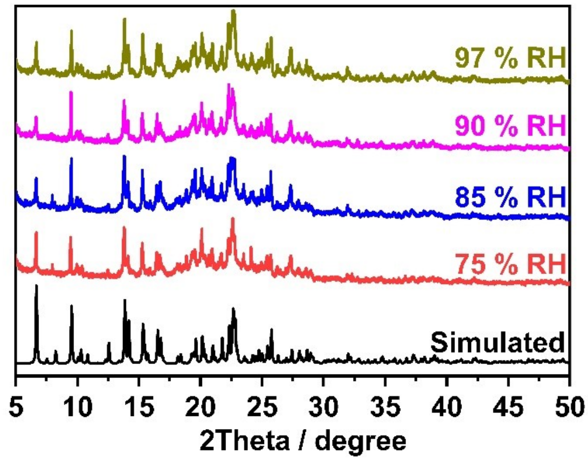

Fig. S12 PXRD patterns of **CUST-751** with different relative humidity.

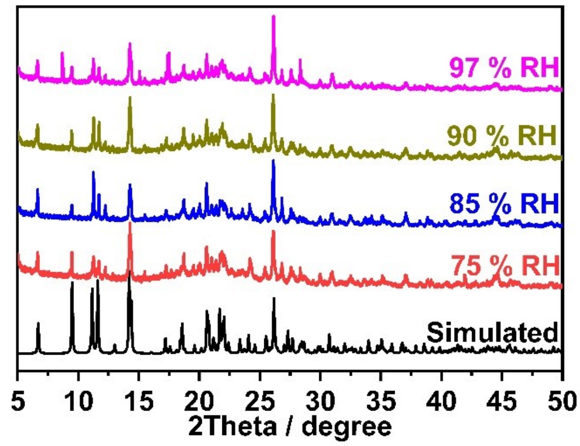

Fig. S13 PXRD patterns of **CUST-752** with different relative humidity.

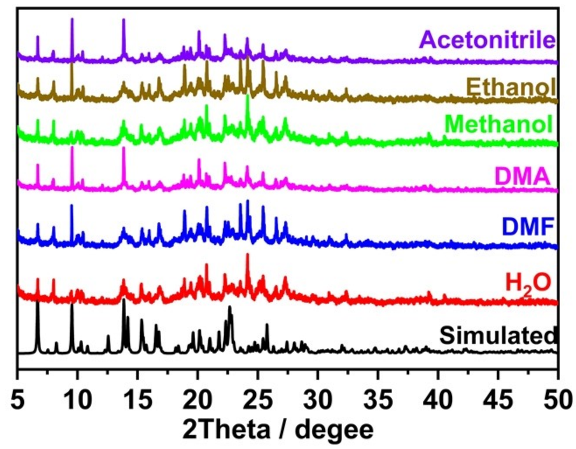

Fig.S14 The PXRD patterns of **CUST-751** in different solvents.

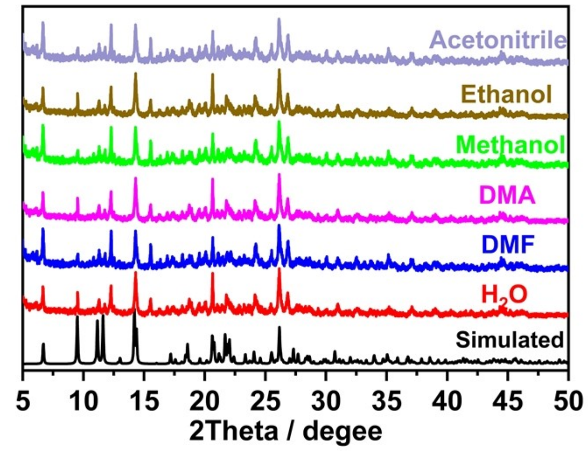

Fig.S15 The PXRD patterns of **CUST-752** in different solvents.

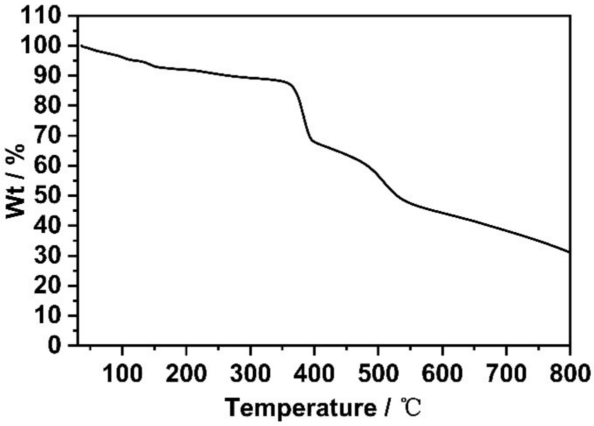

Fig. S16 TGA curve of **CUST-751**.

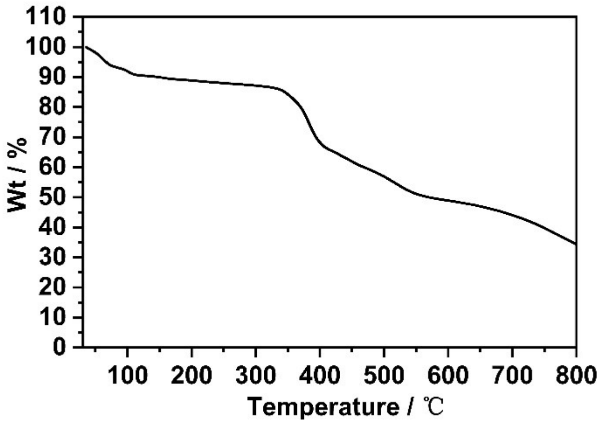

Fig. S17 TGA curve of **CUST-752**.

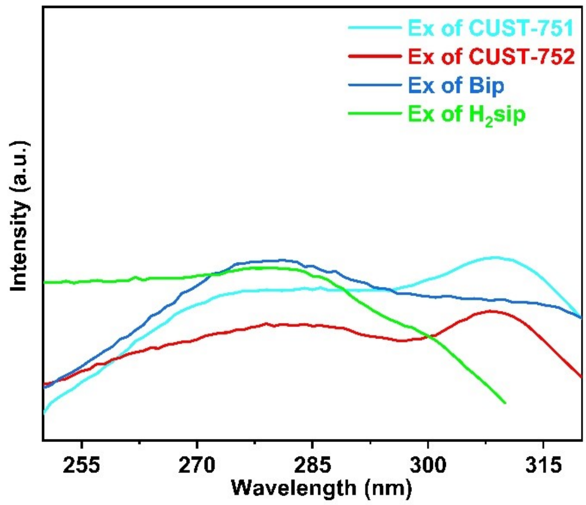

Fig.S18 The solid-state excitation spectra of free ligands and MOFs.

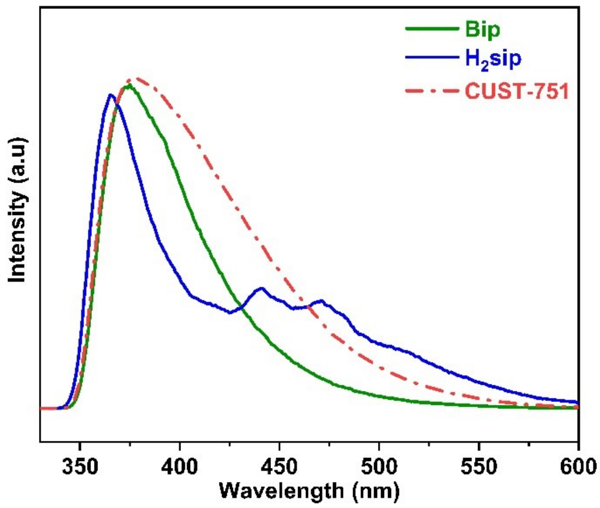

Fig.S19 Fluorescence emission spectrum of free ligands and **CUST-751**.

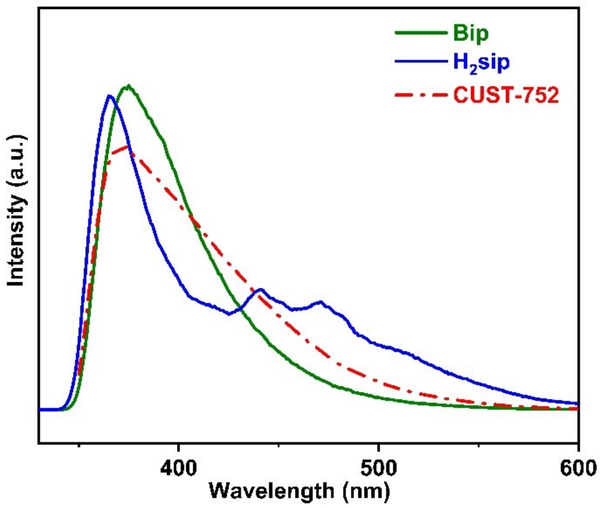

Fig.S20 Fluorescence emission spectrum of free ligands and **CUST-752**.

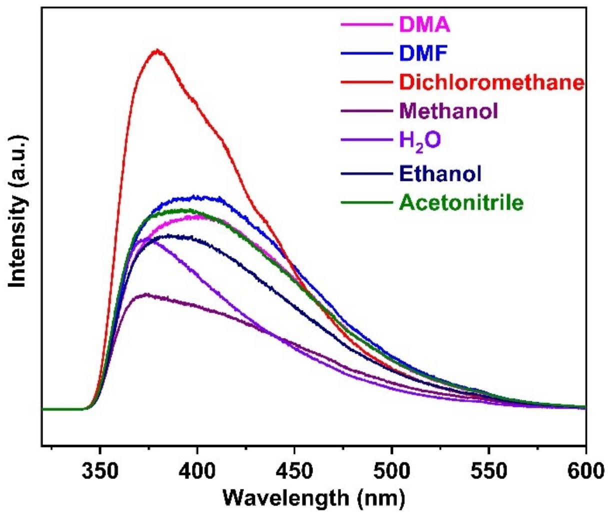

Fig.S21 Photoluminescence spectra of **CUST-751** in different solvents.

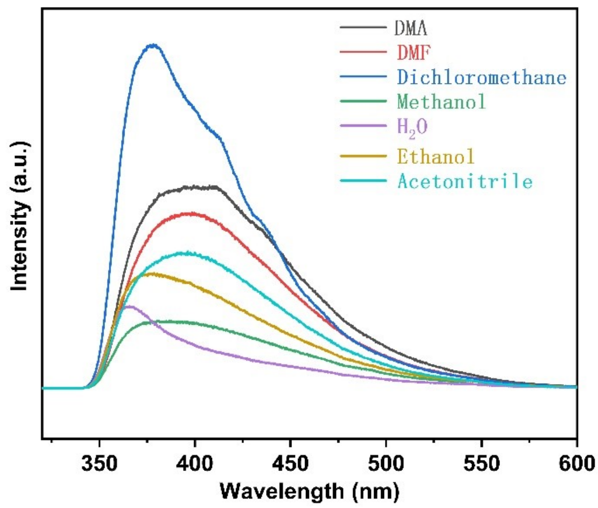

Fig.S22 Photoluminescence spectra of **CUST-752** in different solvents.

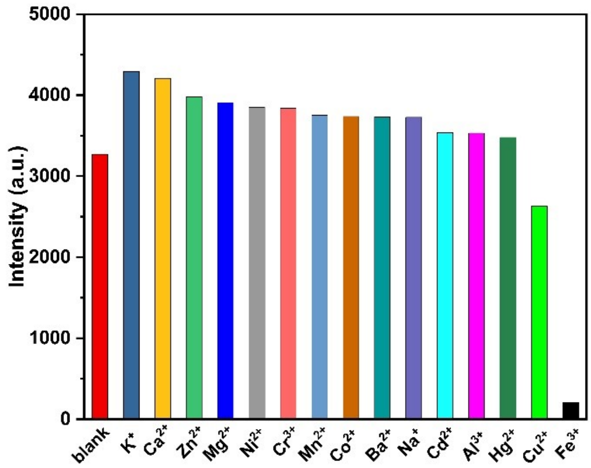

Fig.S23 Emission peak intensity of **CUST-751** in the presence of different metal ions.

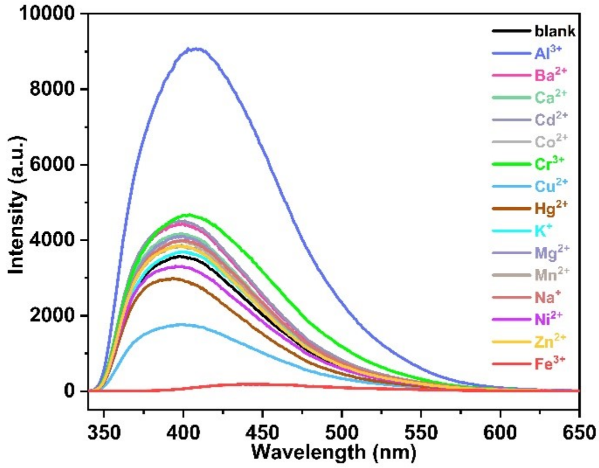

Fig.S24 Emission peak intensity of **CUST-752** in the presence of different metal ions.

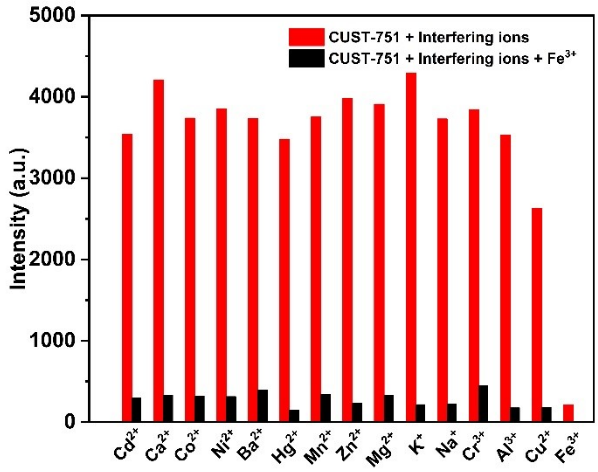

Fig.S25 Selective detection of Fe^{3+} for **CUST-751** in the presence of other interference cations.

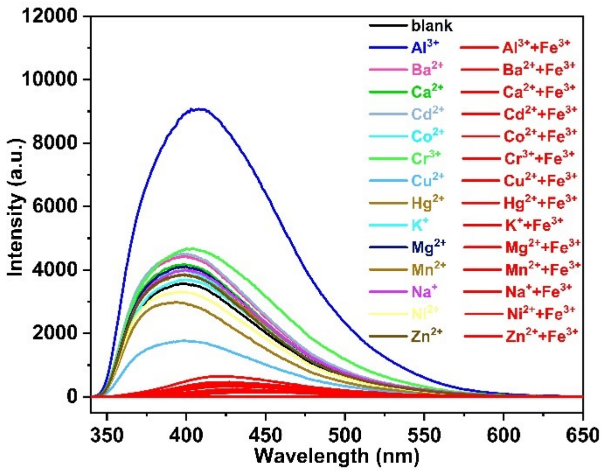

Fig.S26 Selective detection of Fe^{3+} for **CUST-752** in the presence of other interference cations.

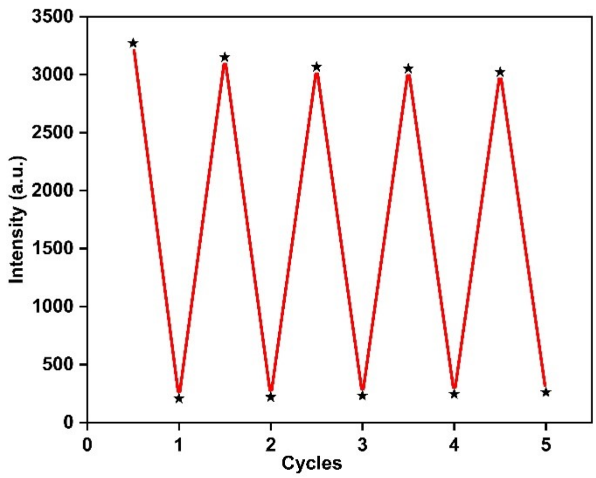

Fig.S27 Recyclability study for the DMF suspension of **CUST-751** towards the sensing of Fe^{3+} ions.

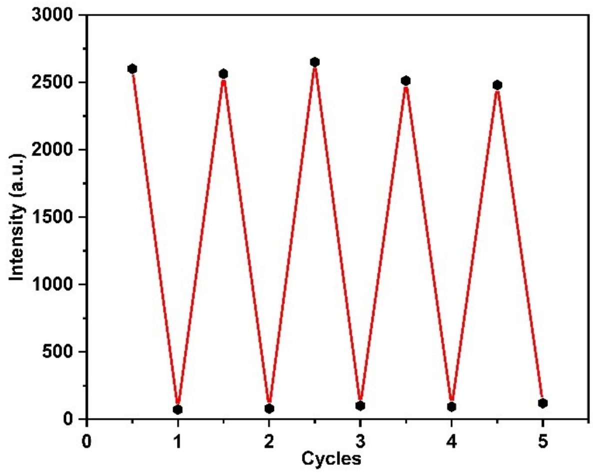

Fig.S28 Recyclability study for the DMF suspension of **CUST-752** towards the sensing of Fe^{3+} ions.

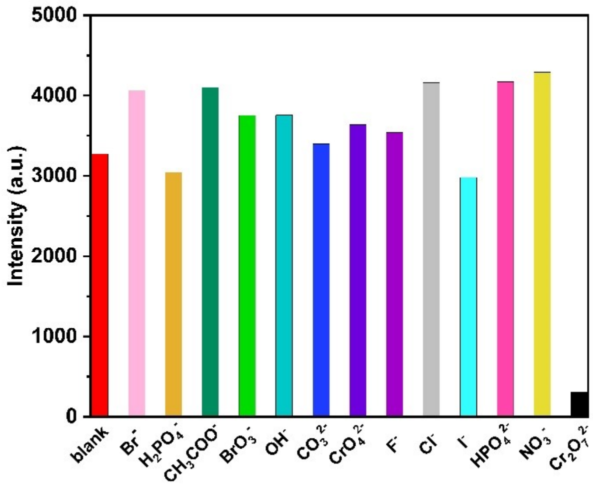

Fig.S29 Fluorescence intensity response of different anions to **CUST-751**.

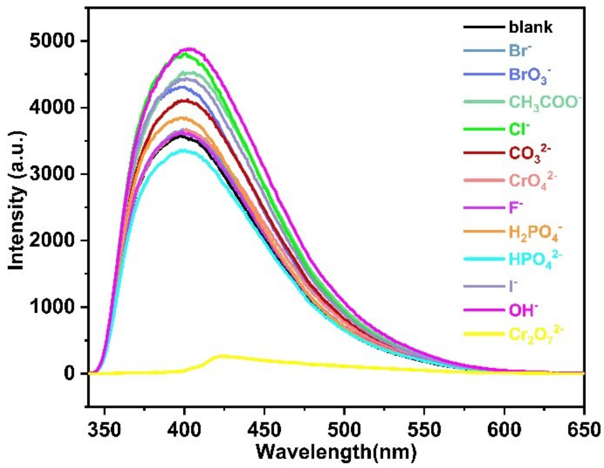

Fig.S30 Fluorescence intensity response of different anions to **CUST-752**.

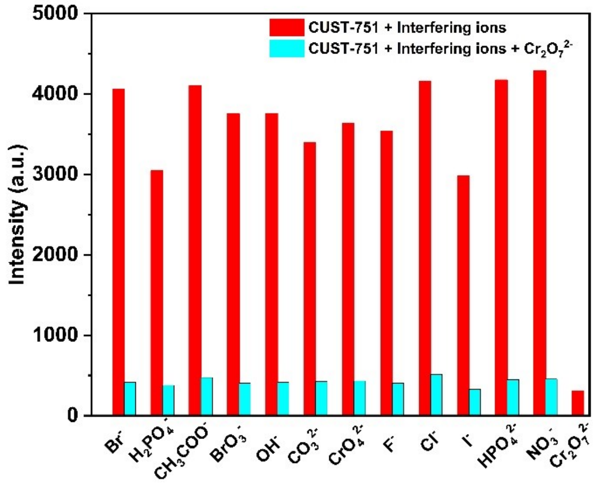

Fig.S31 Fluorescence intensity response of **CUST-751** in the presence of $Cr_2O_7^{2-}$ and other anions.

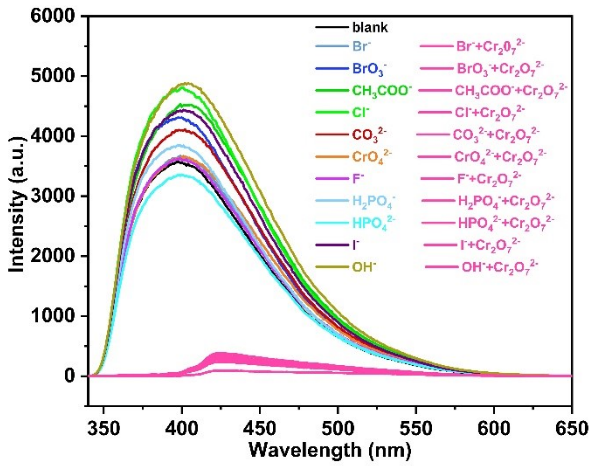

Fig.S32 Fluorescence intensity response of **CUST-752** in the presence of $Cr_2O_7^{2-}$ and other anions.

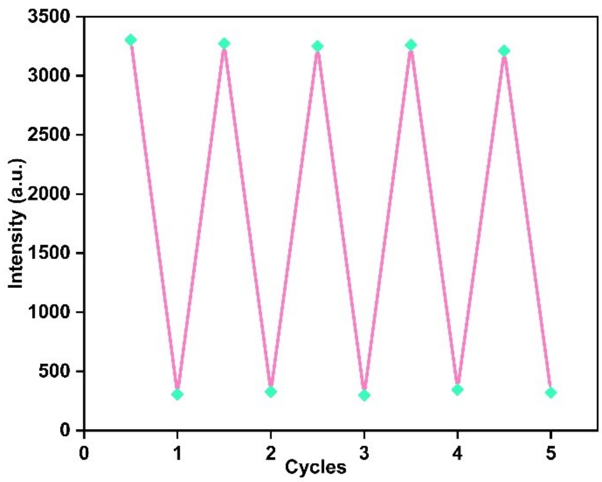

Fig.S33 Five cycle tests of **CUST-751** sensing $Cr_2O_7^{2-}$ ions.

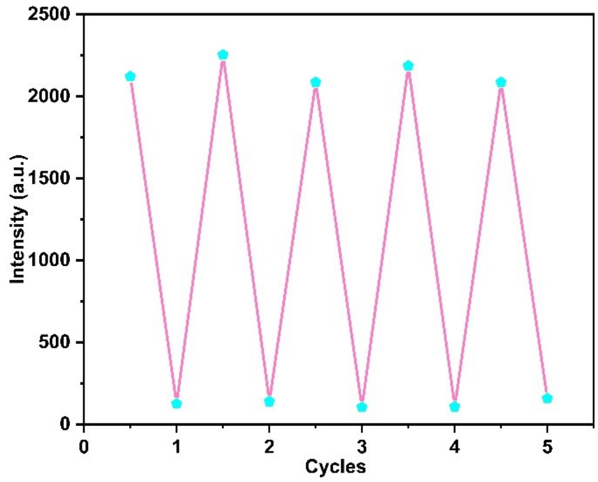

Fig.S34 Five cycle tests of **CUST-751** sensing $Cr_2O_7^{2-}$ ions.

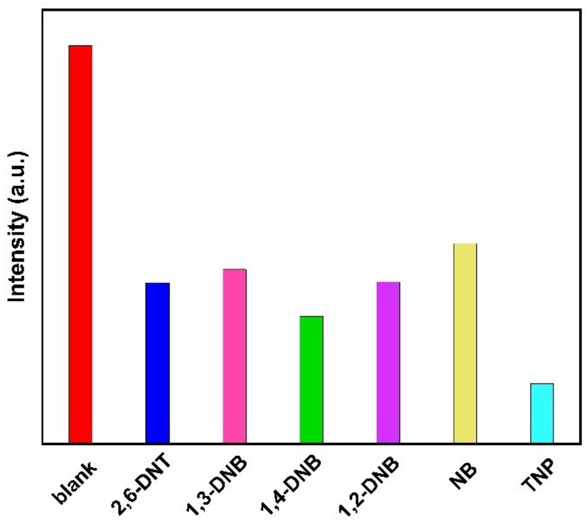

Fig.S35 Fluorescence intensity of **CUST-751** in DMF solutions of different nitroaromatic compounds.

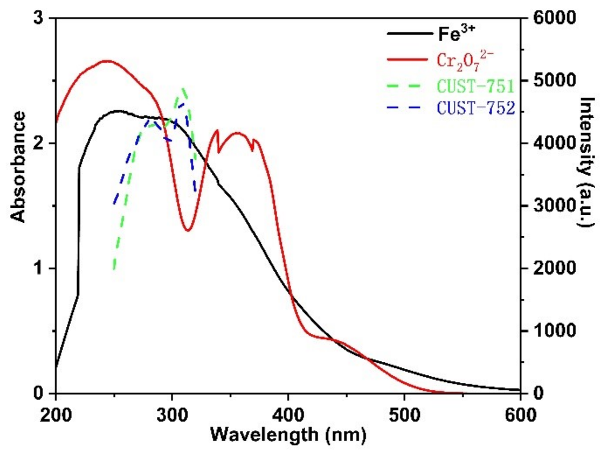

Fig.S36 UV-vis spectra of quenchers with fluorescence excitation spectra of **CUST-751** and **CUST-752**.

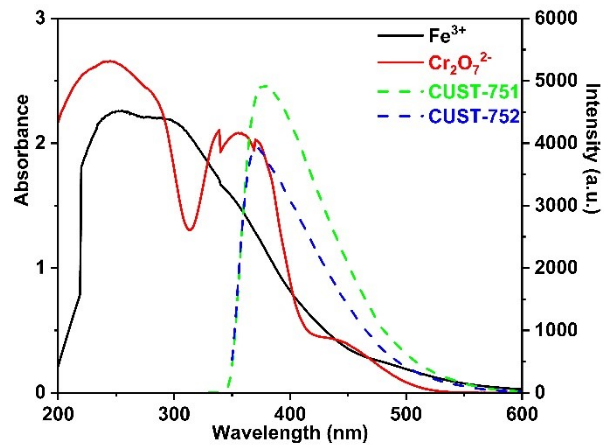

Fig.S37 UV-vis spectra of quenchers with fluorescence emission spectra of **CUST-751** and **CUST-752**.

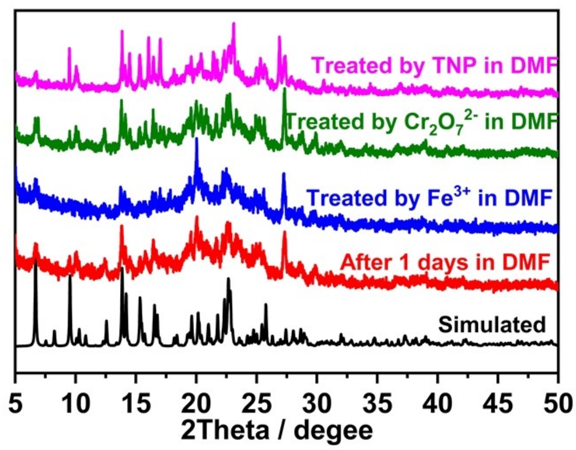

Fig.S38 PXRD patterns of **CUST-751** after immersing in analyte solutions for 24 hours.

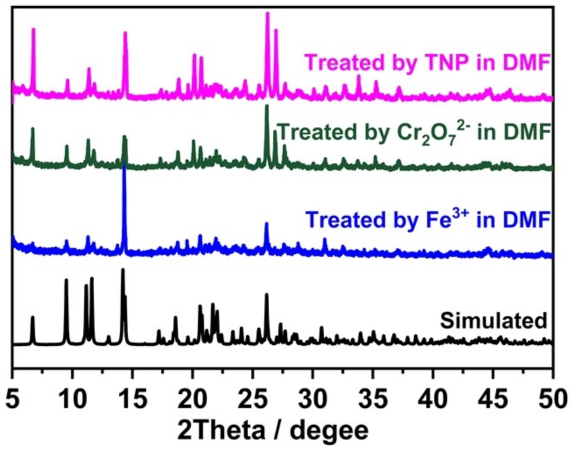

Fig.S39 PXRD patterns of **CUST-752** after immersing in analyte solutions for 24 hours.

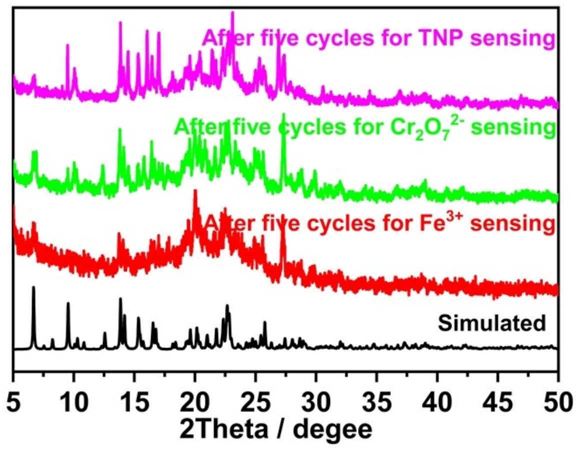

Fig.S40 PXRD patterns of **CUST-751** after five cycles for Fe^{3+}, $Cr_2O_7^{2-}$ and TNP sensing.

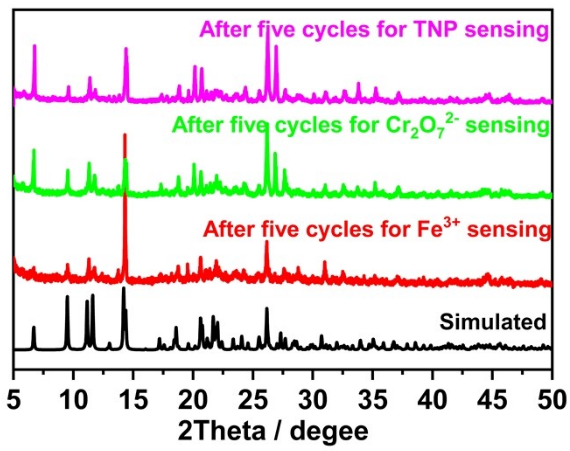

Fig.S41 PXRD patterns of **CUST-752** after five cycles for Fe^{3+}, $Cr_2O_7^{2-}$ and TNP sensing.

Table S3. A summary of the quenching constant for detecting Fe^{3+}/$Cr_2O_7^{2-}$/TNP.

MOF	Quenching Constant (K_{SV}/M^{-1}) for Fe^{3+}	Quenching Constant (K_{SV}/M^{-1}) for $Cr_2O_7^{2-}$	Quenching Constant (K_{SV}/M^{-1}) for TNP	Ref.
CUST-751	$1.27\times10^4M^{-1}$	$1.02\times10^4M^{-1}$	$3.44\times10^4M^{-1}$	**This work**
CUST-752	$8.92\times10^3M^{-1}$	$1.10\times10^4M^{-1}$	---	**This work**
$[Zn_3(dpcp)_2(1,4'\text{-bmib})_2]_n$	$4.06\times10^4M^{-1}$	$5.32\times10^4M^{-1}$	---	[2]
$[Zn(2\text{-ata})(bidpe)]_n]_n$	$5.27\times10^4M^{-1}$	$1.03\times10^5M^{-1}$	---	[2]
$[Cd(dbta)]_n$	$3.47\times10^3M^{-1}$	$3.5\times10^3M^{-1}$	$6.24\times10^3M^{-1}$	[3]
$\{[H_2N(Me)_2]_2[Zn_5(L)_2(OH)_2]\cdot3DMF\}_n$	$9.79\times10^4M^{-1}$	$1.45\times10^4M^{-1}$	---	[4]
$[Zn(L)]\cdot2MeOH\cdot H_2O$	$1.03\times10^4M^{-1}$	$1.18\times10^3M^{-1}$	$3.21\times10^4M^{-1}$	[5]
$[Zn_2(4,4'\text{-nba})_2(1,4\text{-bib})_2]_n$	$1.68\times10^4M^{-1}$	$6.70\times10^3M^{-1}$	---	[6]
$[Cd_3(L)_2(BDC)_6(DMF)_2]$	$4.04\times10^4M^{-1}$	$2.28\times10^4M^{-1}$	$4.29\times10^4M^{-1}$	[7]
$[Cd_3(L)_2(NH_2\text{-BDC})_6(DMF)_2]$	$3.23\times10^4M^{-1}$	$2.33\times10^4M^{-1}$	$3.89\times10^4M^{-1}$	[7]
$[Cd_3(L)_2(Br\text{-BDC})_6(DMF)_2]$	$5.25\times10^4M^{-1}$	$8.18\times10^4M^{-1}$	$7.57\times10^4M^{-1}$	[7]
$[Eu_2(HICA)(BTEC)(H_2O)_2]_n$	$2.03\times10^4M^{-1}$	$1.14\times10^4M^{-1}$	---	[8]
$\{[Tb_2(HICA)(BTEC)(H_2O)_2]\cdot2.5H_2O\}_n$	$1.20\times10^4M^{-1}$	$8.23\times10^3M^{-1}$	---	[8]
$\{[Zn(IPA)(L)]\}_n$	---	$1.37\times10^3M^{-1}$	$2.16\times10^4M^{-1}$	[9]

References

[1]. Z. Pahlevanneshan, M. Moghadam, V. Mirkhani, S. Tangestaninejad, I. Mohammadpoor-Baltork and S. Rezaei, *New J. Chem.*, 2015, **39**, 9729-9734.

[2]. W. Liu, N. Li, X. Zhang, Y. Zhao, Z. Zong, R. X. Wu, J. P. Tong, C.F. Bi, F. Shao and Yu. H Fan, *Cryst. Growth Des.,* 2021, **21**, 5558−5572.

[3]. L. Liu, Y. Jia, D. Li and M. Hu, *New J. Chem.*, 2022, **46**, 8636-8643.

[4]. Y. T. Yan, Y. l. Wu, L. N. Zheng, C. Wei, P. F. Tang, W. P. Wu, W. Y. Zhang and Y. Y.

Wang, *New J. Chem.*, 2022, **46**, 4292-4299.

[5]. Q. Sun, K. Yang, W. Ma, L. Zhang and G. Yuan, *Inorg. Chem. Front.*, 2020, **7**, 4387-4395.

[6]. T. Y. Xu, J. M. Li, Y. H. Han, A. R. Wang, K. H. He and Z. F. Shi, *New J. Chem.*, 2020, **44**, 4011-4022.

[7]. M. Y. Fan, H. H. Yu, P. Fu, Z. M. Su, X. Li, X. L. Hu, F. W. Gao and Q. Q. Pan, *Dyes Pigm.*, 2021, **185**, 108834.

[8]. H. Yu, M. Fan, Q. Liu, Z. Su, X. Li, Q. Pan and X. Hu, *Inorg. Chem.*, 2020, **59**, 2005-2010.

[9]. B. Parmar, Y. Rachuri, K. K. Bisht, R. Laiya and E. Suresh, *Inorg. Chem.*, 2017, **56**, 2627-2638.